Research Article

Alexander S. Gusev*, Elena V. Shimanovskaya, Nikolai I. Shatsky, Firouz Sakhibov,
Anatoly E. Piskunov, and Nina V. Kharchenko

Stellar population in star formation regions of galaxies

Abstract: We developed techniques for searching young unresolved star groupings (clusters, associations, and their complexes) and of estimating their physical parameters. Our study is based on spectroscopic, spectrophotometric, and *UBVRI* photometric observations of 19 spiral galaxies. In the studied galaxies, we found 1510 objects younger than 10 Myr and present their catalogue. Having combined photometric and spectroscopic data, we derived extinctions, chemical abundances, sizes, ages, and masses of these groupings. We discuss separately the specific cases, when the gas extinction does not agree with the interstellar one. We assume that this is due to spatial offset of H II clouds with respect to the related stellar population. We developed a method to estimate age of stellar population of the studied complexes using their morphology and the relation with associated Hα emission region. In result we obtained the estimates of chemical abundances for 80, masses for 63, and ages for 57 young objects observed in seven galaxies.

Keywords: H II regions, star formation, star clusters, photometry, spiral galaxies

1 Introduction

Estimating the physical parameters, such as age, mass, size, metallicity of young extragalactic stellar groupings in star forming (SF) regions, is important for understanding of star formation and early evolution of star clusters in outer galaxies. Usually one understands under a star forming region a single conglomerate of young star clusters, dust clouds, and ionized gas. Hα emission from H II region is a good indicator of young stellar population there. Star clusters without Hα emission are definitely older than 10 Myr.

Corresponding Author: Alexander S. Gusev: Sternberg Astronomical Institute, Lomonosov Moscow State University, Universitetsky pr. 13, 119992 Moscow, Russia; Email: gusev@sai.msu.ru
Elena V. Shimanovskaya, Nikolai I. Shatsky: Sternberg Astronomical Institute, Lomonosov Moscow State University, Universitetsky pr. 13, 119992 Moscow, Russia
Firouz Sakhibov: University of Applied Sciences of Mittelhessen, Campus Friedberg, Department of Mathematics, Natural Sciences and Data Processing, Wilhelm-Leuschner-Strasse 13, 61169 Friedberg, Germany
Anatoly E. Piskunov: Institute of Astronomy, Russian Academy of Sciences, ul. Pyatnitskaya 48, 119017 Moscow, Russia
Nina V. Kharchenko: Main Astronomical Observatory, National Academy of Sciences of Ukraine, ul. Zabolotnogo 27, 03680 Kiev, Ukraine

SF regions have a hierarchical structure over a large range of scales. Meantime the youngest star clusters with diameters of a few parsecs and OB associations with diameters of several tens of parsecs occupy smallest scales, the older clusters form larger structures. The largest coherent SF regions are star complexes with diameters of order of $\sim$500-600 pc (Elmegreen & Efremov 1996; Efremov & Elmegreen 1998). The sizes of the largest complexes can reach 2 kpc (Elmegreen et al. 1996). Their sizes are limited only by the effective thickness of the galactic gaseous discs. Star complexes are groups of young stars, associations, and clusters. We study, in this paper, SF regions with sizes from $\sim$ 30 to $\sim$ 1000 pc.

We consider, in this paper, stellar groupings in SF regions in not very distant galaxies (see Table 1). Our angular resolution $\sim$ 1 − 1.5 arcsec corresponds to linear resolution of about 30–40 pc in the nearest galaxies NGC 628, NGC 5585, and NGC 6946 only, and to 350–400 pc in the most distant galaxy NGC 783. This means that we are not able to separate young star clusters and OB associations even in the nearest galaxies where they will be observed as star-like objects. In more distant galaxies, we can observe SF regions with sizes of 200–300 pc and larger, *i.e.* star complexes. We will use the common term "star cluster" for the studied stellar populations in SF regions in the paper. It should be realized that this term covers young ob-

jects of different types: star complexes, cluster complexes, stellar aggregates, OB associations, and star clusters.

A SF region evolves during the first tens Myr of its life through several evolutionary stages, from a stage when young stars are completely obscured by their dusty gas cocoons to a stage of a young star cluster with no evidence of the ionized gas (Lada & Lada 2003). Evolutionary classification scheme of star clusters was presented in (Whitmore et al. 2011) and is based on *Hubble Space Telescope (HST)* observations of M83. Star clusters become visible in optical bands since about 1 Myr. Ionized gas stays spatially coincident with cluster stars during 1–4 Myr. Clusters with ages ≈ 4–5 Myr have a small H II bubble with a radius of 7–20 pc, surrounding the cluster (Whitmore et al. 2011). Young star groups with ages ≥ 5 Myr have a larger ionized gas bubble surrounding the cluster. In this paper we only study the clusters and complexes with ages ∼ 1 − 10 Myr, *i.e.* objects with Hα emission, which are visible in optical wavelengths or (when Hα data are absent), the objects with colour indices typical to stellar populations younger than 10 Myr.

A study of the earliest stages of young stellar groups is a difficult task because of impact of gas and dust. Understanding of this impact on observations of extragalactic complexes is very important for the interpretation of multicolour photometry in terms of parameters of evolutionary synthesis models, such as initial mass function and star formation history. A lot of spectroscopic and of photometric observations of extragalactic H II regions and of extragalactic SF regions have been performed during last decades. However, these observations are carried out separately. Whereas if one uses a combination of spectroscopic and photometric data, one can eliminate a problem of degeneracies between age and extinction, or age and metallicity. These degeneracies present a hurdle for the analysis of photometric data (Scalo 1986). Also, the impact of gas contribution to the total photometric flux can be accounted for (see compilations in (Reines et al. 2010)).

Keeping in mind the degeneracy problem we started several years ago simultaneous spectroscopic and photometric observations of SF regions in nearby galaxies. Here we should mention also the progress in the solution of the degeneracies achieved by coupling the spectroscopy with *UBVI* photometry of star clusters in M82 in (Konstantopoulos et al. 2009). Unlike to our study however, the authors of (Konstantopoulos et al. 2009) use the absorption spectra, and in result have considered relatively old star clusters only.

The spectroscopic data itself plays an important role in the study of the chemical evolution of galaxies, where oxygen and nitrogen are key elements. These aspects of the application of our spectral observations, as well as of

the data reduction, are summarised in our previous papers (Gusev et al. 2012, 2013).

This paper contains the results presented at the conference "Modern stellar astronomy – 2017". See papers (Gusev et al. 2016) (Sections 5 and 6), and (Gusev et al. 2018) (Sections 2–4) for more detailed description of the data, and of its analysis.

2 Observational data

The sample of galaxies is based on our photometric survey of 26 galaxies (Gusev et al. 2015), 19 of them contain SF regions. The sample is presented in Table 1, where data on the Galactic absorption, $A(B)_{Gal}$, is taken from the NED[1] database, and the other parameters are taken from the LEDA[2] database (Paturel at al. 2003). The morphological type of the galaxy is given in column (2), the apparent and absolute magnitudes are listed in columns (3) and (4), the inclination and position angles are given in columns (5) and (6), and the isophotal radii in arcmin and kpc are listed in columns (7) and (8). The adopted distances are given in column (9). The Galactic absorption and the dust absorption due to the inclination of a galaxy are presented in columns (10) and (11). Finally, a presence of broadband photometric (Ph) and Hα observations of the galaxies and spectrophotometric and spectroscopic (Sp) data for the SF regions and the references to them are given in column (12). The adopted value of the Hubble constant is equal to $H_0 = 75$ km s^{-1}Mpc^{-1}.

2.1 Earlier published data

Most of our own observations were published earlier (see the notes in Table 1). The analysis of photometric (*UBVRI*) data is given in (Gusev et al. 2015) and in references therein. Spectrophotometric Hα (Hα+[N II]) observations were described in (Gusev & Kaisin 2002; Gusev & Efremov 2013; Gusev et al. 2016). The results of spectroscopic observations of 102 H II regions in seven galaxies were presented in (Gusev et al. 2012, 2013).

These data were used for deriving of the intrinsic photometric parameters and for estimation of the physical parameters of SF regions (Sections 5 and 6.2).

Additionally, we used FITS images of galaxies in broadband photometric passbands and Hα line, which

---

1 http://ned.ipac.caltech.edu/
2 http://leda.univ-lyon1.fr/

Table 1. The galaxy sample.

Galaxy	Type	B_t (mag)	M_B^a (mag)	i (degree)	PA (degree)	R_{25}^b (arcmin)	R_{25}^b (kpc)	D (Mpc)	$A(B)_{Gal}$ (mag)	$A(B)_{in}$ (mag)	Data^c
1	2	3	4	5	6	7	8	9	10	11	12
NGC 245	SA(rs)b	12.72	−21.12	21	145	0.62	9.6	53.8	0.097	0.04	Ph
NGC 266	SB(rs)ab	12.27	−21.94	15	95	1.55	28.7	63.8	0.252	0.01	Ph+Hα
NGC 628	SA(s)c	9.70	−20.72	7	25	5.23	11.0	7.2	0.254	0.04	Ph+Hα+Sp
NGC 783	Sc	13.18	−22.01	43	57	0.71	14.6	70.5	0.222	0.45	Ph+Sp
NGC 2336	SAB(r)bc	11.19	−22.14	55	175	2.51	23.5	32.2	0.120	0.41	Ph+Hα+Sp
NGC 3184	SAB(rs)cd	10.31	−19.98	14	117	3.79	11.3	10.2	0.060	0.02	Ph+Hα+Sp
NGC 3726	SAB(r)c	10.31	−20.72	49	16	2.62	10.9	14.3	0.060	0.30	Ph+Hα+Sp
NGC 4136	SAB(r)c	11.92	−18.38	22	30	1.20	2.8	8.0	0.066	0.05	Ph+Sp
NGC 5351	SA(r)b	12.57	−21.16	60	101	1.20	17.8	51.1	0.074	0.40	Ph+Sp
NGC 5585	SAB(s)d	10.94	−18.73	53	34	2.13	3.5	5.7	0.057	0.38	Ph+Hα+Sp
NGC 5605	(R)SAB(rs)c	12.58	−20.86	36	65	0.81	10.6	44.8	0.318	0.15	Ph
NGC 5665	SAB(rs)c	12.25	−20.42	53	151	0.95	8.6	31.1	0.091	0.35	Ph
NGC 6217	(R)SB(rs)bc	11.89	−20.45	33	162	1.15	6.9	20.6	0.158	0.22	Ph+Hα+Sp
NGC 6946	SAB(rs)cd	9.75	−20.68	31	62	7.74	13.3	5.9	1.241	0.04	Ph+Hα+Sp
NGC 7331	SA(s)b	10.20	−21.68	75	169	4.89	20.1	14.1	0.331	0.61	Ph+Hα+Sp
NGC 7678	SAB(rs)c	12.50	−21.55	44	21	1.04	14.5	47.8	0.178	0.23	Ph+Sp
NGC 7721	SA(s)c	11.11	−21.18	81	16	1.51	11.6	26.3	0.121	0.98	Ph
IC 1525	SBb	12.51	−21.89	48	27	0.97	19.7	69.6	0.410	0.24	Ph
UGC 11973	SAB(s)bc	13.34	−22.47	81	39	1.73	29.7	58.8	0.748	0.85	Ph

^{a} Absolute magnitude of a galaxy corrected for Galactic extinction and inclination effects.

^{b} Radius of a galaxy at the isophotal level 25 mag arcsec^{-2} in the B band corrected for Galactic extinction and inclination effects.

^{c} References: NGC 245 – *UBVRI* photometry (Gusev et al. 2015);

NGC 266 – *UBVRI* photometry (Gusev et al. 2015), Hα+[N ii] image (Epinat et al. 2008);

NGC 628 – *UBVRI* photometry (Bruevich et al. 2007), Hα+[N ii] image (Gusev & Efremov 2013), Hα, Hβ, [N ii], and [O iii] spectrophotometry (Belley & Roy 1992), 3D spectroscopy (Rosales-Ortega et al. 2011), spectroscopy (McCall et al. 1985; Ferguson et al. 1998; van Zee et al. 1998; Bresolin et al. 1999; Cedrés et al. 2012; Gusev et al. 2012; Sánchez et al. 2012; Berg et al. 2013, 2015);

NGC 783 – *UBVRI* photometry (Gusev 2006a,b), spectroscopy (Gusev et al. 2012);

NGC 2336 – *UBVRI* photometry (Gusev & Park 2003), Hα+[N ii] image (Young et al. 1996), spectroscopy (Gusev et al. 2012);

NGC 3184 – *BVRI* photometry (Gusev & Kaisin 2002), *U* photometry (Larsen & Richtler 1999), Hα image (Gusev & Kaisin 2002), spectroscopy (McCall et al. 1985; van Zee et al. 1998; Sánchez et al. 2012), SDSS;

NGC 3726 – *BVRI* photometry (Gusev et al. 2002), *UBV* photometry (this work, see Section 2.2), Hα+[N ii] image (Knapen et al. 2004), spectroscopy (SDSS);

NGC 4136 – *BVRI* photometry (Gusev et al. 2003), spectroscopy (SDSS);

NGC 5351 – *BVRI* photometry (Gusev & Kaisin 2004), *UBV* photometry (this work, see Section 2.2), spectroscopy (Márquez et al. 2002), SDSS;

NGC 5585 – *UBVRI* photometry (Bruevich et al. 2010), Hα+[N ii] image (Dale et al. 2009), spectroscopy (SDSS);

NGC 5605 – *BVRI* photometry (Artamonov et al. 2000);

NGC 5665 – *BVRI* photometry (Artamonov et al. 2000);

NGC 6217 – *UBVRI* photometry (Artamonov et al. 1999; Gusev et al. 2015), Hα+[N ii] image (Epinat et al. 2008), spectroscopy (Gusev et al. 2012);

NGC 6946 – *UBVRI* photometry (Gusev et al. 2015), Hα+[N ii] image (Gusev et al. 2016), Hα, Hβ, [N ii], and [O iii] spectrophotometry (Belley & Roy 1992), 3D spectroscopy (García-Benito et al. 2010), spectroscopy (McCall et al. 1985; Ferguson et al. 1998; Cedrés et al. 2012; Gusev et al. 2013);

NGC 7331 – *UBVRI* photometry (Gusev et al. 2015), *BVRI* photometry (Regan et al. 2004), Hα+[N ii] image (Gusev et al. 2016), spectroscopy (Bresolin et al. 1999; Gusev et al. 2012);

NGC 7678 – *UBVR* photometry (Artamonov et al. 1997), *UBVRI* photometry (Gusev et al. 2015), spectroscopy (Gusev et al. 2012; Ann & Kim 1996);

NGC 7721 – *UBVRI* photometry (Gusev et al. 2015);

IC 1525 – *UBVRI* photometry (Bruevich et al. 2011);

UGC 11973 – *UBVRI* photometry (Gusev et al. 2015).

were taken from the NED database, and spectroscopic data from the Sloan Digital Sky Survey DR13[3], as well as from the literature (see references in Table 1). The absolute calibration of these images was carried out using the parameters of descriptors from the original FITS files (images) and their explanations (Larsen & Richtler 1999; Regan et al. 2004; Knapen et al. 2004; Dale et al. 2009; James et al. 2004; Kennicutt et al. 2008; Young et al. 1996; Epinat et al. 2008; Schmitt et al. 2006).

These data were used for identification and selection of SF regions (Section 3) and calculation of their photometric fluxes (Section 4).

We also found the data of spectrophotometry in emission lines, integral field spectroscopy, and long-slit spectroscopy for SF regions in the galaxies of our sample from the literature and SDSS (see notes in Table 1). These data were used for additional identification of young star groups in the galaxies in Section 3.

2.2 New observations and data reduction

Additionally, we carried out photometric observations of two galaxies of our sample.

UBV observations of NGC 3726 and NGC 5351 were done on June 12, 2016 using a newly installed 2.5 m telescope of the Caucasus Observatory of Sternberg Astronomical Institute at the Mt. Shatzhatmaz (Kornilov et al. 2016), with a CCD camera at the Cassegrain f/8 focus. A CCD camera manufactured by Niels Bohr Institute based on E2V CCD230-42 detector (pixel size $15\mu m$), and a set of standard Bessel *UBV* filters were used. The camera was cooled with liquid nitrogen. The chip size, 2048×2064 pixels, provides a field of view of 5.3×5.3 arcmin^2, with an image scale of 0.155 arcsec pixel^{-1}. The journal of observations is given in Table 2.

The filters together with the CCD detector form a photometric system, which is close to the standard Johnson-Cousins *UBV* system.

The data reduction was carried out using standard techniques, with the ESO-MIDAS[4] image processing system. The main image reduction stages were described in (Gusev et al. 2015) (see also references therein).

The translation of the instrumental *ubv* magnitudes to the standard Johnson-Cousins *UBV* system was carried out using the following colour equations:

$$U = u + (0.2432 \pm 0.0076)(u - b)- \tag{1}$$

$$- (0.5419 \pm 0.0603)M(z) + (23.2685 \pm 0.0084)$$
$$B = b + (0.1117 \pm 0.0193)(b - v)-$$
$$- (0.3067 \pm 0.0176)M(z) + (26.2187 \pm 0.0160)$$
$$V = v - (0.0739 \pm 0.0209)(b - v)-$$
$$- (0.2034 \pm 0.0152)M(z) + (26.2904 \pm 0.0167),$$

where $M(z) \equiv \sec z$ is an airmass and z is a zenith distance. These equations were constructed using observations of standard photometric stars from the fields PG 1528+062 and PG 1530+057 (Landolt 1992), acquired on the same nights. In addition, the published aperture photometry in *B* and *V* bands for both galaxies from the LEDA database was used for the absolute calibration of the galaxies. Finally, we compared images of NGC 3726 and NGC 5351 in the *B* and *V* filters with those obtained in (Gusev et al. 2002; Gusev & Kaisin 2004). The galaxies were not previously observed in *U* passband, thus we estimated the absolute calibration in *U* using the position of the galaxies in colour-colour diagram $(U - B) - (B - V)$. We found, that within errors of colour equation for *U*, the galaxies lie on the normal colour sequence for galaxies. The zero-point errors were found to be: $\Delta U = 0.04$ mag, $\Delta B = 0.02$ mag, and $\Delta V = 0.015$ mag.

Table 2. Journal of observations.

Galaxy	Filter	Exposures (s)	Seeing (arcsec)	Airmass
NGC 3726	U	400×3	1.7	2.57
	B	200×3	1.4	2.81
	V	180×3+60	1.6	1.36
NGC 5351	U	300×4	1.1	1.23
	B	180×3	1.1	1.19
	V	180×3+10	1.0	1.16

3 Search and identification of young stellar groupings

3.1 Preliminary selection

For the preliminary selection of star clusters we identified bright star-like regions in the galaxies using their *B* and Hα images. The identification was carried out using the SExtractor[5] program.

---

3 http://www.sdss.org/dr13/
4 http://www.eso.org/sci/software/esomidas/

5 http://sextractor.sourceforge.net/

The galactic images were preliminarily prepared for the processing with the SExtractor procedure. Firstly, we smoothed the images using a median filter with a window of 11×11 pixels^2. In the second step, we subtracted the smoothed images from the original ones. Finally, we smoothed the resulting images using an average filter with a window of 5×5 pixels^2. Field stars were deleted from the images. Obtained *B* images of 19 galaxies and Hα images of 9 galaxies were processed using the SExtractor code.

We used default parameters of SExtractor with two changes. A detection threshold of 5σ above the local background and the number of pixels ≥ 10 above the threshold were adopted. In present study we excluded nuclei of galaxies from consideration, because physical conditions of star formation in the nuclear regions differ significantly from the conditions of star formation in the discs.

The application of the technique resulted in the detection of 4233 candidates for star clusters in 19 galaxies. We also detected 3351 H II regions in 9 galaxies based on processing of Hα (Hα+[N II]) images.

3.2 Young star groupings candidates and morphology of surrounding ionized hydrogen emission

As we mentioned in Introduction, the morphology of the ionized gas can be used as star cluster age indicator. To our regret we are not able to study the Hα morphology directly at scale of 40–50 pc and smaller as authors of (Whitmore et al. 2011), who used *HST* observational data, do. However, as we showed in (Gusev et al. 2016) the distance between photometric centres of star clusters and Hα emission correlates within a single SF region with the relation between A(gas) or A(stars) and depends from the age. Thus it can be used as an evolutionary indicator.

Distributions of separations of H II regions and the nearest to them cluster candidate are shown in Figure 1. Here we use two samples of H II regions. The first sample (top panel of Figure 1) contains 691 H II regions in NGC 628, NGC 3184, and NGC 6946 from large Hα surveys (Berg et al. 2015; Cedrés et al. 2012; Sánchez et al. 2012). The second sample (bottom panel of Figure 1) includes 3351 H II regions in 9 galaxies detected via SExtrartor from Hα images in present study. In Figure 2 we show for the same 9 galaxies the distributions of the separations of the centers of *B* images of young star clusters and of the nearest Hα regions. This sample contains 3783 objects.

As it is seen from Figures 1, 2, the most of the possible pairs are very close to each other with a distance to be less than 1.5 arcsec. This corresponds for the most abundant
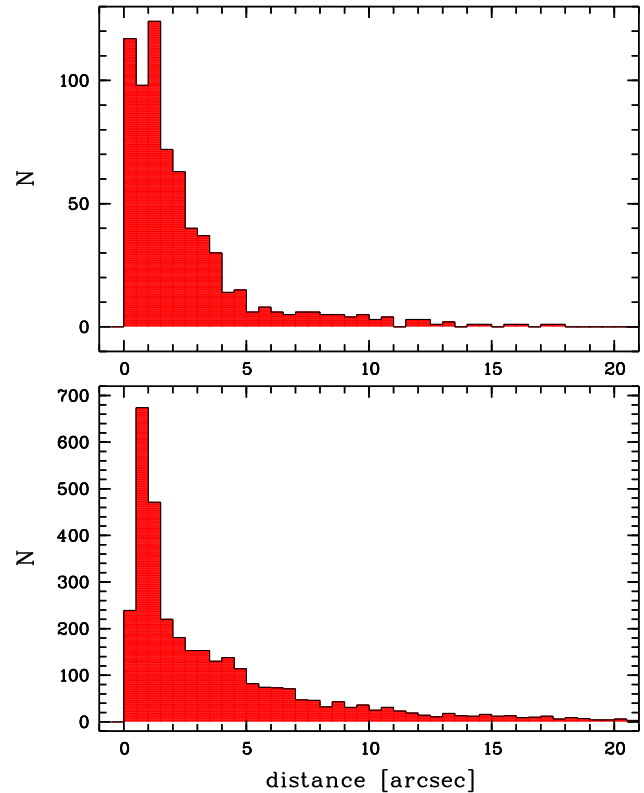

Figure 1. Distributions of separations of H II regions and centers of *B* images of the nearest star clusters. Samples of H II regions from (Berg et al. 2015; Cedrés et al. 2012; Sánchez et al. 2012) in NGC 628, NGC 3184, and NGC 6946 are shown in the top panel, and those obtained via SExtrartor in this study in the bottom one.
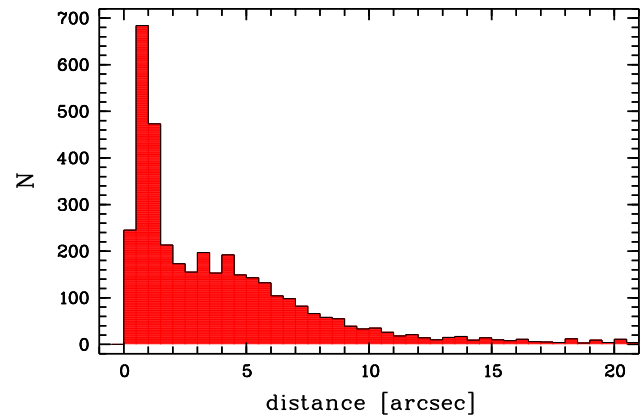
Figure 2. Distributions of separation of the star cluster *B* images as derived by SExtractor, and nearest H II regions.

with our objects galaxies NGC 628 and NGC 694 to the linear distance of $\approx 45 - 50$ pc.

The greater part of the objects is separated at 1.5 to 5-7 arcseconds (Figure 1 or Figure 2). This is seen more clear in Figure 2, where the distribution has a plateau at separations from 1.5 to 6 arcsec. Probably, this plateau is
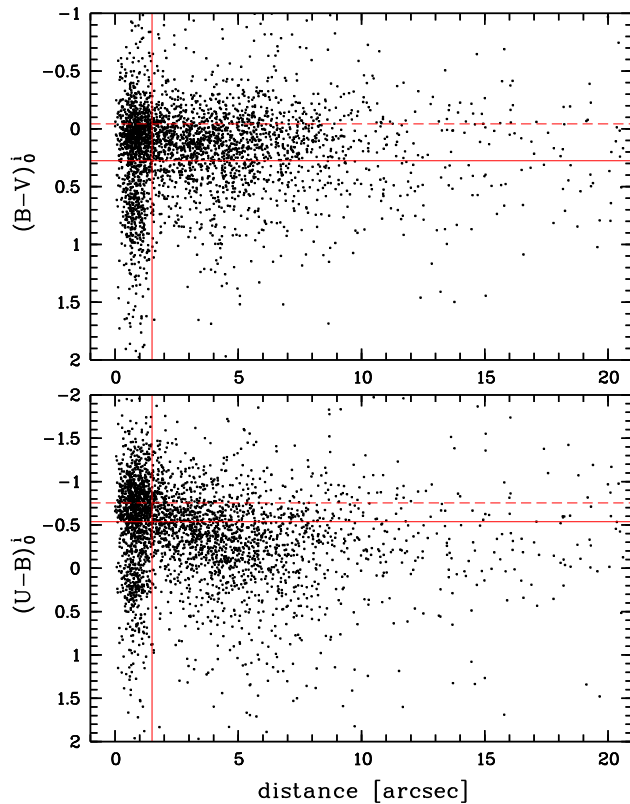
Figure 3. Colour indices $U - B$ (top) and $B - V$ (bottom) of star clusters, corrected for Galactic extinction and inclination effects, vs. separation of its *B*-image and the nearest H ɪɪ region. Vertical lines correspond to the separation of 1.5 arcsec. Solid horizontal lines are maximum colour indices of stellar cluster models with age of ≤ 10 Myr, meantime dashed horizontal lines are minimum colour indices of the models of the same age.

a result of expanding of star formation from of ∼ 100 to ∼ 700 pc (Efremov & Elmegreen 1998). Within such complexes we can observe older star clusters without Hα emission (ages > 10 Myr) and neighbouring young H ɪɪ regions without visible radiation in the *U* and *B* passbands ("emerging clusters" according to (Whitmore et al. 2011) with ages ∼ 3 Myr). Most objects with minimum distances more than 7 arcsec seems are not related to each other; they have a random distribution.

The relation between colour indices of young star cluster candidates and their separations is given in Figure 3. The sample used here is the same as in Figure 2. Fluxes from star clusters in the *U*, *B*, and *V* bands were measured within a round aperture with the 2.5 arcsec radius. The local background was subtracted from the flux, measured inside the round aperture. For the background, we took the average flux from the area of ring with inner and outer radii of 5 and 7.5 arcsec, respectively.

The diagrams in Figure 3 support our above speculations, about Figure 2. Clusters with close Hα emission sources (closer than 1.5 arcsec), have a wide range of colours, from extremely blue to extremely red. Star clusters from the plateau region have more uniform colours. We do not observe here the objects with extremely red colour indices. Note a correlation between cluster $U - B$ colour index, and the separating distance to the H ɪɪ region (bottom panel of Figure 3): with increase of the separations the clusters become redder. A duration of star formation in SF complexes at large spatial scales (500-1000 pc) is about 30 Myr (Efremov & Elmegreen 1998). Among star clusters within a complex, one can meet both very young and intermediate-age objects (∼ 100 Myr). The colour indices of stellar groupings in Figure 3 correspond to the range from several Myr to several hundred Myr (see Figure 4). We did not find any correlation between the separation with H ɪɪ regions and colours of star clusters for objects with Hα-cluster separation larger than 7 arcsec.

We believe that a significant absorption is observed only in young tight cluster-H ɪɪ region couples (separations less than < 1.5 arcsec). Star clusters without Hα emission have the absorption close to zero (Whitmore et al. 2011). As a result, we observe "red" star clusters with Hα emission, but do not see extremely red clusters which are located farther than 1.5 arcsec from H ɪɪ regions. Note that lack of extremely red clusters distant from Hα regions can be a result of selection effect due to smaller sample of wider pairs and consequently of smaller probability to have the extreme colours. Anyway, red colours of star clusters with and without Hα emission have different reasons (absorption in the first case and red stellar population in the second).

Note that one meets the objects located far from Hα sources, but having blue colours. Colour indices $U - B < -0.7$ mag and $B - V < 0$ mag are typical for young stellar populations with ages < 7 − 8 Myr. (Figure 4).

The detailed analysis of the distributions in Figure 3 of wide cluster − Hα region pairs is of interest, but lies to our regret outside the goals and objectives of this study.

We present variations of colour indices and integrated magnitudes of aging synthetic stellar systems and their evolutionary tracks in the colour-age, magnitude-age and colour-colour diagrams in Figures 4 and 5, respectively. Here we use a grid of isochrones provided by the Padova group (Bertelli et al. 1994; Bressan et al. 2012; Girardi et al. 2000; Marigo & Girardi 2007; Marigo et al. 2008) via the online server CMD[6].

---

6 http://stev.oapd.inaf.it/cgi-bin/cmd/
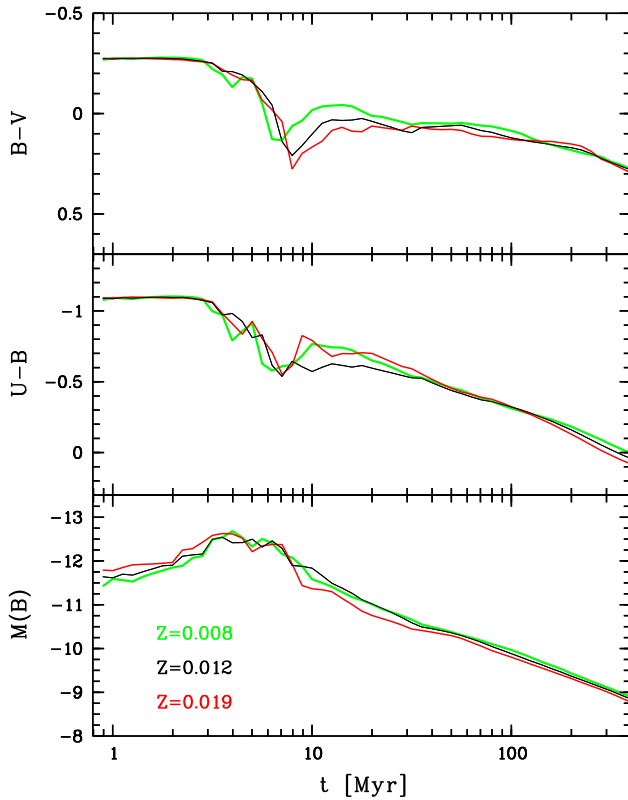
Figure 4. Variations of colour indices $U - B$ (top), $B - V$ (middle), and absolute magnitude (bottom) of synthetic stellar systems with $M = 10^5 M_\odot$ and $Z = 0.008, 0.012$, and 0.019 vs age.

As one can see from Figures 4 and 5, the models considerably change their colours during the age interval of the interest (10 Myr), though there is no strong dependence of colour indices on age at the first 3 Myr of cluster life. After 6 – 7 Myrs evolutionary tracks form loops in the colour-colour diagram $(U - B) - (B - V)$ (Figure 5). The ambiguity of age estimation from $U - B$ exists for models with ages between 6 and 40 Myr (the middle panel of Figure 4). At the same time, the luminosity of stellar models drops down significantly beginning from $t \approx 7$ Myr. Clusters lose ≈ 2 mag in B from $t = 6$ to ≈ 50 Myr (bottom panel of Figure 4). Since absorption in star clusters older than 6 Myr is insignificant (Whitmore et al. 2011), the most objects with $-0.75 < (U - B)_0^i < -0.5$ are young stellar systems ($t \leq 10$ Myr) due to the selection effects.

As a result, for further more detailed consideration we selected cluster candidates satisfying the following conditions: (i) those, which form tight couples with nearest H II regions, *i.e.* are separated by less than 1.5 arcsec (in 9 galaxies with obtained Hα+[N II] (Hα) images), (ii) with measured emission spectra (in 13 galaxies with obtained spectroscopic data), (iii) which have $(U - B)_0^i < -0.537$ mag (in 16 galaxies with obtained U images), (iv)
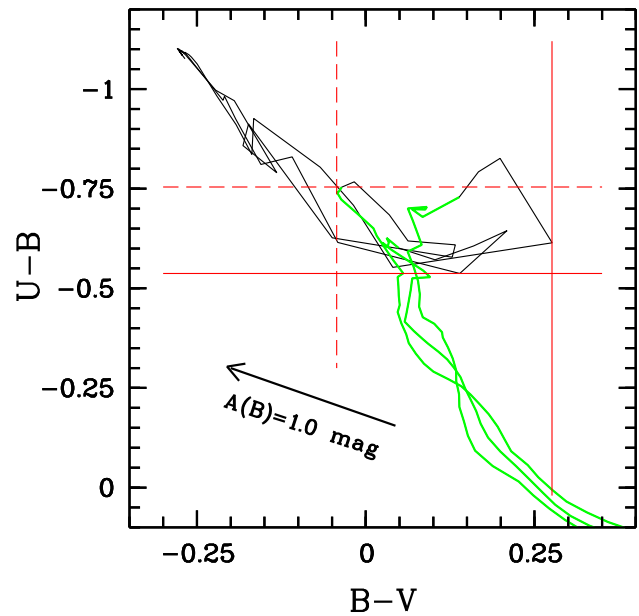
Figure 5. Evolutionary tracks of synthetic stellar systems with $Z = 0.008, 0.012$, and 0.019. Thin black curves are tracks of SSP systems younger than 10 Myr, thick green (gray in BW colours) curves are tracks of SSP systems older than 10 Myr. Extinction vector is shown. The solid and dashed lines indicate the same as in Figure 3.

which have $(B-V)_0^i < -0.043$ mag (in NGC 4136, NGC 5605, NGC 5665, and outer part of NGC 7331). In total, we chose 2578 objects.

3.3 Evolutionary classification scheme for star clusters

Returning to the evolutionary classification scheme of star clusters (Whitmore et al. 2011), we can adjust it for ground observations data with the resolution of $\sim$ 1 arcsec. Figures 6, 7 illustrate the evolutionary sequence of young SF regions. The youngest SF regions have the Hα emission, but they are not visible in the U and B passbands (see the left maps in Figures 6 and 7). These regions correspond to the last stage of obscured clusters and to emerging clusters with ages $t \sim 1$ Myr (Whitmore et al. 2011).

In the next stage, we observe optical radiation from stars in U and B bands that is coincident with ionized gas emission (the second maps from the left in Figures 6 and 7). These star clusters are emerging or very young clusters by classification scheme of (Whitmore et al. 2011), they have ages $t \approx 1 - 5$ Myr.

From older clusters we observe Hα emission in a large bubble surrounding a star cluster (the third maps in Figures 6 and 7). A spatial displacement between photomet-
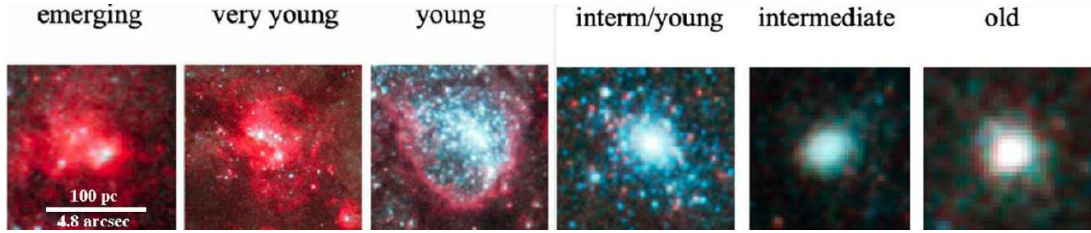
Figure 6. Evolutionary classification of star clusters (Whitmore et al. 2011). This figure is a copy of original Figure 1 from (Whitmore et al. 2011).

Figure 7. Hα images of star formation regions in NGC 3184 with superimposed isophotes in the *U* band. 22.0, 21.7, 21.4, and 21.1 mag arcsec^{-2} isophotes are shown. Galactocentric coordinates of centres of the images are presented. The size of the images is 9.5×9.5 arcsec^2. North is upwards and east is to the left.

ric (stellar) and gas emission centres is observed in such objects (Figure 7). This stage was classified in (Whitmore et al. 2011) as a stage of young clusters. Their ages are from $4-5$ to $8-10$ Myr.

Next, we observe blue clusters without any gas emission (fourth map from the left in Figure 6 and right map in Figure 7). This stage begins since $t \approx 8-10$ Myr. Later, they begin to redden slowly, but retain their morphology (see two right maps in Figure 6). They are classified as young/intermediate-age, intermediate-age and old clusters in (Whitmore et al. 2011).

4 Catalogue of photometric parameters of star forming regions

The obtained young star cluster database is used for more detailed study (see Section 3.2). First of all, to characterize typical size of the SF regions d we derived the geometric mean of the major and minor axes of the cluster: $d = \sqrt{d_{max} \times d_{min}}$. The technique of the measurements is described in (Gusev et al. 2016).

The measurements of apparent total *B* magnitude and colour indices $U-B$, $B-V$, $V-R$, and $V-I$ were made within round aperture. For selection of the aperture size we used the data on d_{max} and on the seeing.

The catalogue of SF regions in 19 studied galaxies is presented in electronic form at http://lnfm1.sai.msu.ru/~gusev/sfr_cat.html. The first version of the catalogue contains photometric parameters for 1510 objects including data on 101 SF regions with obtained spectra from (Gusev et al. 2016). Columns of the catalogue present the following data:

(1) serial number;

(2) galaxy name (NGC, IC, or UGC);

(3) serial number of the object within a galaxy;

(4, 5) apparent coordinates in the plane of the sky, with respect to the galaxy centre (arcseconds, positive values correspond to the northern (4) and western (5) positions);

(6, 7) deprojected galactocentric distances in units of kpc (6) and in units of isophotal radius (7), corrected for the Galactic extinction and inclination effects;

(8) apparent total *B* magnitude;

(9) absolute magnitude M_B, $M_B = B - 5 \log D - 25$, where D is an adopted distance in units of Mpc;

(10) magnitude uncertainties;

(11–18) apparent colour indices $U-B$ (11), $B-V$ (13), $V-R$ (15), and $V-I$ (17) with their uncertainties (12, 14, 16, 18);

(19, 20) logarithm of spectrophotometric Hα+[N II] flux (19) and its uncertainty (20);

(21) absolute magnitude $M(B)_0^i$, corrected for the Galactic extinction and inclination effects;

(22–25) the colour indices $(U-B)_0^i$ (22), $(B-V)_0^i$ (23), $(V-R)_0^i$ (24), and $(V-I)_0^i$ (25), corrected for the Galactic extinction

and inclination effects;

(26) logarithm of spectrophotometric Hα+[N ɪɪ] flux, corrected for the Galactic extinction and inclination effects, $F(\text{H}\alpha+[\text{N ɪɪ}])_0^i$;

(27) R–Hα index, $R - \text{H}\alpha = R + 2.5 \log F(\text{H}\alpha+[\text{N ɪɪ}])$, where R is in magnitudes, and $F(\text{H}\alpha+[\text{N ɪɪ}])$ is the flux in units of erg s^{-1}cm^{-2};

(28) gas/stars morphology (2 – optical radiation from stars coincides with ionized gas emission, 1 – photometric (stellar) radiation centre is displaced from gas emission centre, 0 – no gas emission, –1 – no Hα data);

(29–53) are reserved for spectral and physical parameters (see Tables 4 and A1 in (Gusev et al. 2016));

(54) estimated diameter in units of pc;

(55) structure of the region (1 – separate object with star-like profile, 2 – double object, 3 – triple object, 4 – separate object with diffuse profile, 5 – ring structure, 6 – complex structure (more than three separate objects), 10...60 – the same as 1...6, but the object is a brighter part (core) of an more extended star forming region).

The photometric errors in the catalogue correspond to the uncertainties of the aperture photometry. A main source of photometric errors is the uncertainty of the galactic background.

For verification of our photometric calibration we used results of study of young star clusters in several nearby galaxies (Larsen 1999, 2004). We identified 38 objects from the list (Larsen 1999, 2004), which are in common with the objects studied here. Unfortunately due to different apertures and seeings we can compare our photometry and data from (Larsen 1999, 2004) qualitatively only. The comparison shows that the systematic deviations in the case of $U - B$ and $B - V$ lie within the data accuracy limit ≤ 0.1 mag with correlation coefficients $r_{U-B} = 0.92$ and $r_{B-V} = 0.94$. In the case of $V - I$ there is negative systematic deviation ≈ 0.20 mag with smaller correlation coefficient $r_{V-I} = 0.83$, and we had to remove this bias with linear regression $V - I = (V - I)_{\text{obs}} + 0.20$. These corrected $V - I$ colour indices are given in the catalogue.

5 Obtaining the "true" photometric parameters

5.1 Gas/stellar absorption and gas contribution

An algorithm of correction of the observed photometric fluxes, and of obtaining of true photometric parameters free from gas contribution, and corrected for interstellar absorption, is described in detail in (Gusev et al. 2016) for 102 SF regions in seven galaxies. It is based on the combination of spectroscopic and multiband photometric observations of SF regions. We mention below two key steps only.

First of all, we assume that emission from stars embedded in the H ɪɪ region is absorbed in the same way as emission in lines of ionized hydrogen surrounding the star groups from the H ɪɪ region, *i.e.* the light extinction for the stars is equal to the extinction in ionized gas $A(\text{stars}) = A(\text{Balmer})$ (or $A(\text{stars}) = A(\text{gas})$). This condition is correct for very young ($t < 5 - 6$ Myr) star clusters (see the second maps from the left in Figures 6 and 7).

Using this assumption, the measured *UBVRI*Hα fluxes have been corrected for interstellar reddening based on Hα/Hβ ratio. We note here that the errors in the absorption estimates obtained from spectroscopic data give the main contribution to the uncertainty of the true colour indices.

Secondly, we corrected the broadband fluxes corresponding to *UBVRI*-photometry for the nebular emission. We determine the relative contributions of the stellar continuum, nebular continuum, and emission lines to the total observed flux in a broadband filter following (Sakhibov & Smirnov 1990). Having obtained in (Gusev et al. 2012, 2013) the emission line ratios for every SF region in our spectroscopic sample, we derived the characteristic values of the electron temperatures and metallicities in the H ɪɪ regions. We used spectrophotometric Hα fluxes (Gusev et al. 2016) for the absolute calibration of the emission line fluxes derived through spectroscopy. Finally, we estimated the relative contributions of the nebular continuum, using the equations for the continuum emission near the limits of the hydrogen series, free-free, and two-photon emissions, given in (Lang 1978; Kaplan & Pikelner 1979; Brown & Mathews 1970; Osterbrock 1989). The contribution from the nebular line emission was computed through the summation of the emission line intensities that appear in a given photometric band. The fluxes for the non-measured emission lines were computed from the derived estimations of the emission measures, using the equations given in (Kaplan & Pikelner 1979; Osterbrock 1989). A total of 18 main emission lines were taken into account.

Figure 8 shows the distributions of the studied SF regions over the relative contribution of the nebular emission to the U, B, and V fluxes. The figure shows that the number of objects decreases with an increase of the relative gas contributions.

As we found in (Gusev et al. 2016) the objects where the contribution of nebular emission is greater than 40% of the total flux do not satisfy the condition $A(\text{stars}) =$
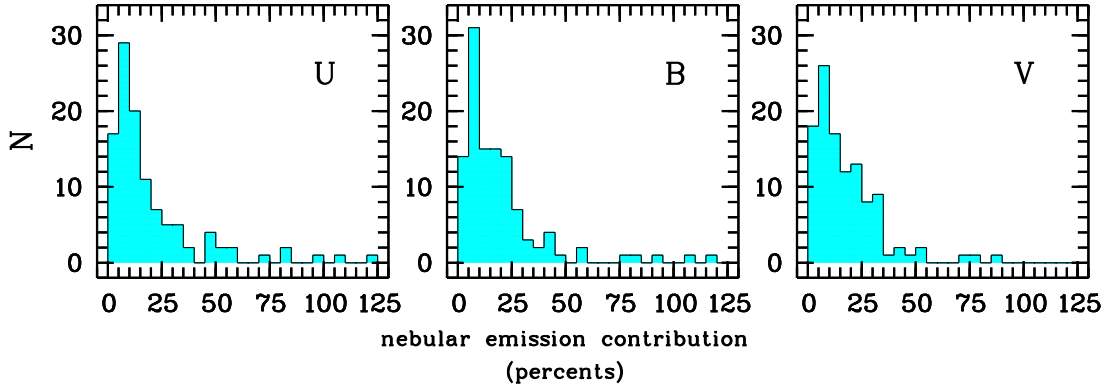
Figure 8. Distributions of studied SF regions over nebular emission contribution in the *U* band (left), in the *B* band (centre), and in the *V* band (right).

A(gas). Thus, we eliminate 13 objects with extremely high nebular emission contribution (> 40%) in the *B* and/or *V* passbands from further consideration in Section 6.2.

5.2 Equivalent widths and spectrophotometric fluxes

A relation between the equivalent width EW(Hα) and the fluxes in Hα line and *R* band is a good indicator of agreement of spectroscopic, spectrophotometric, and photometric fluxes.

In Figure 9 we compare the equivalent width EW(Hα) with the ratio of the Hα flux to the pure stellar emission flux (corrected for the gas contribution as described in Section 5.1) in the *R* band for the studied objects. The EW(Hα) data were taken from (Gusev et al. 2012, 2013).

Figure 9 shows that most objects (black squares) follow linear regression (solid line):

$$\log \mathrm{EW}(\mathrm{H}\alpha) = \log \frac{F(\mathrm{H}\alpha)}{F(R_{\mathrm{stars}})} + (3.15 \pm 0.05),$$

where the value of the constant 3.15 ± 0.05 is in good agreement with the effective bandwidth (1580Å) of the *R* filter (Bessell 1990).

Objects with unreasonable equivalent widths EW(Hα) > 1500Å and with unreasonable ratios $F(\mathrm{H}\alpha)/F(R_{\mathrm{stars}})$ > 1 were not taken into account in the computation of the linear regression.

The extreme characteristics of these objects may indicate spatial deviation between the photometric centres of the ionized gas and the stellar group associated with it. In such cases, the slit of the spectrograph crosses the centre of the H II region, but covers the edge of the star cluster only (see the sample in Figure 7).
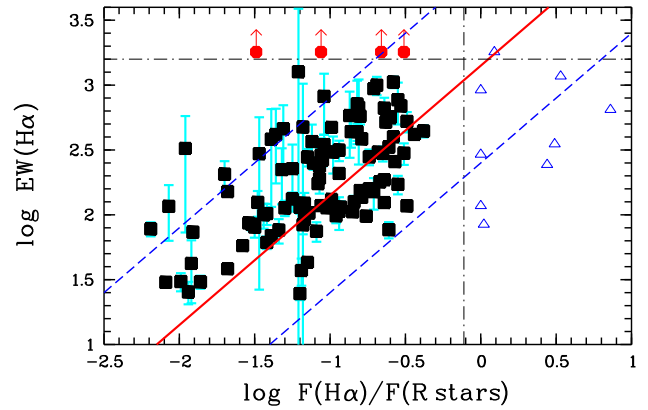
**Figure 9.** Diagram $\log F(\mathrm{H}\alpha)/F(R_{\mathrm{stars}})$ versus $\log \mathrm{EW}(\mathrm{H}\alpha)$ for the SF regions. Dot-dashed lines are upper limits of the equivalent width EW(Hα) (horizontal line) and of the ratio of the Hα- to star emission-fluxes in *R* band (vertical line), computed in (Reines et al. 2010). Red thick line is a linear fit, computed for SF regions (black squares), located under the upper limits of the EW(Hα) and $F(\mathrm{H}\alpha)/F(R_{\mathrm{stars}})$ (horizontal and vertical dot dashed lines). Upper and lower 95% prediction limits of the linear fit are also shown (dashed lines). Objects with an unreasonable EW(Hα) > 1500Å (red circles) and with an unreasonable ratio $F(\mathrm{H}\alpha)/F(R_{\mathrm{stars}})$ > 1 (blue triangles) are marked.

6 The results

6.1 Two-colour diagrams and comparison with synthetic models

In Figure 10 we compare the observed photometric properties of the star groups with simple stellar population (SSP) tracks using Salpeter IMF with a mass range from 0.1 to 100$M_\odot$. For the track computation we use the *Standard* SSP modes according to the technique described in (Piskunov at al. 2011).
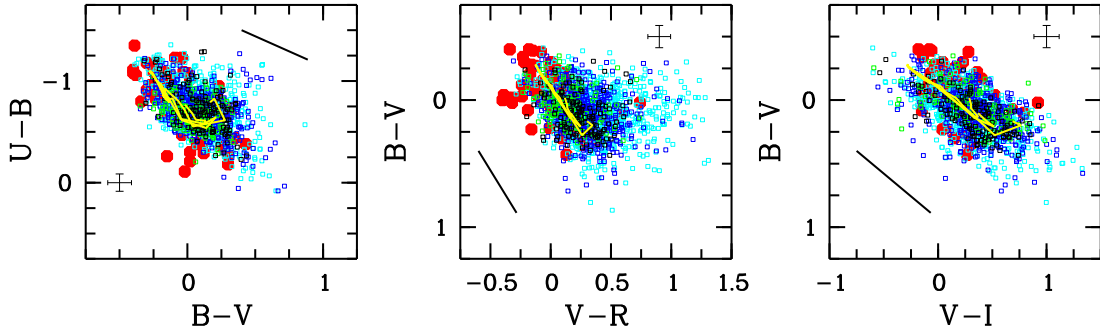
Figure 10. Colour–colour diagrams $(U - B) - (B - V)$, $(B - V) - (V - R)$, and $(B - V) - (V - I)$ for star clusters in the studied galaxies for (i) true colour sample (red filled circles), and (ii) the colours corrected for the Galactic absorption and the dust absorption due to the inclination of a galaxy for star clusters in which radiation from stars coincides spatially with Hα emission (cyan dots), clusters with a displacement between stellar and gas radiation (blue dots), objects with absence of gas emission (green dots), and star clusters with absence of Hα data (black dots). Yellow lines show SSP models with continuously populated IMF with Salpeter slope $\alpha = -2.35$ and $Z = 0.008$, 0.012, and 0.019. The black straight line in the corner of the diagrams is parallel to the extinction vector. The mean accuracy of the true colours of star clusters are shown by error bars.

We consider two samples of the SF regions. The first sample includes 63 objects with true colour indices. It is based on the sample of 102 SF regions (Gusev et al. 2016) except the objects with extremely high nebular emission contributions (Section 5.1), the objects with unreasonable EW(Hα) and $F(H\alpha)/F(R_{stars})$ (Section 5.2), and objects with large errors of $A(V)$ estimations ($\Delta A(V) > 0.8$ mag). The second sample includes remaining 1447 objects described in Section 4. For SF regions from the second sample we use the colours corrected for the Galactic absorption and the dust absorption due to the inclination of a galaxy.

Figure 10 plots SSP model tracks in the two-colour diagrams. They are superimposed over: (i) objects with true colours (SF regions in which A(stars) = A(gas) condition is satisfied), (ii) objects in which radiation from stars coincides spatially with Hα emission, objects with a displacement between stellar and gas radiation sources, and objects with absence of gas emission. Mean errors of the true colour indices are: $\Delta(U - B) = 0.09$, $\Delta(B - V) = 0.11$, $\Delta(V - R) = 0.08$, $\Delta(V - I) = 0.15$ (Figure 10), mean errors of the colour indices corrected for the Galactic absorption and the inclination of a galaxy for 1447 objects are: $\Delta(U - B) = 0.09$, $\Delta(B - V) = 0.09$, $\Delta(V - R) = 0.09$, $\Delta(V - I) = 0.12$.

Star clusters without Hα emission (*i.e.* they have not an additional absorption) are concentrated in the area of the models with ages of 7-10 Myr. Among objects with detected Hα emission we have find SF regions, both close to the SSP tracks, and displaced with respect to SSP models along the extinction vector to the lower right corner of the diagrams.

6.2 Physical parameters of SF regions

Multicolour photometry provides a useful tool for constraining the physical parameters of star clusters in SF regions. Here we use the method of the minimisation of "observed minus computed" $(O - C)$ parameters, described in (Gusev et al. 2007, 2016).

We use as "observed parameters" the derived true colours and luminosities, which are corrected for the light extinction and for the nebular emission. The procedure of derivation of ages (t) and masses (m) of star clusters in SF regions can be divided into the following steps. First, the SSP models, computed for the derived from spectroscopy chemical abundance, are presented as a grid of colour indices and luminosities for a broad range of variation of searching parameters $t(i)$ and $m(j)$, with indices i, and j to be the numbers of rows and columns of the grid. The step of the table along $\log(t)$ is 0.05 dex. The step along $\log(m)$ depends on the interval of luminosity variations of SR regions in a given galaxy:

$$h_{\log(m)} = (\log(m_{max}) - \log(m_{min}))/N,$$

where N is the number of the evolutionary tracks. For every node (i, j), we calculate value of the $(O-C)_{i,j}$. At the second step we search for the node with minimum value of $(O - C)_{i,j}$.

The major source of rather low accuracies of the age estimations, especially for small ages ($t < 3$ Myr), where the colour gradients of age are very flat is the uncertainty introduced by the light absorption, and by gas emission contribution corrections.

We were able to estimate ages for 57, and masses for 63 star clusters of 102 SF regions with obtained spectra
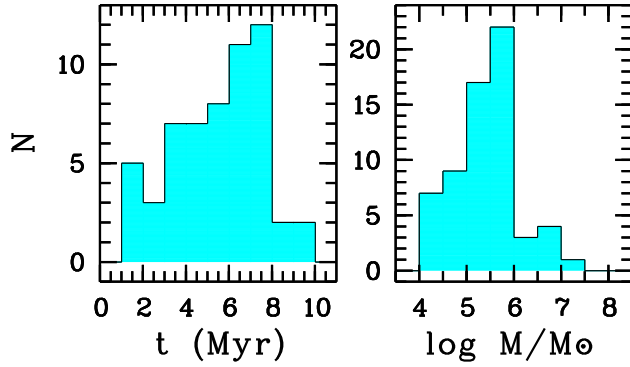
Figure 11. Distributions of star clusters over age (left panel), and mass (right panel) in 7 studied galaxies.

observed in seven galaxies. We believe that the condition $A(\text{gas}) = A(\text{stars})$ is valid for these objects. For six of them the age estimations have been obtained with low accuracies, the errors exceed the range of 1-8 Myr.

Left histogram in Figure 11 shows the age distribution of 57 SF regions in studied galaxies. The shape of the distribution can be explained by selection effects. Very young star clusters have high extinction. Old clusters and complexes ($t > 8$ Myr) have no Hα emission.

Right histogram in Figure 11 shows that the masses of the star clusters range from $10^4 M_\odot$ in the nearby galaxies NGC 628 and NGC 6946 to $10^7 M_\odot$ in distant galaxy NGC 7678; however, most of them have masses $10^5 - 10^6 M_\odot$.

6.3 Extragalactic SF regions and Milky Way open clusters

We investigate the existence of the evolutionary relation between star clusters embedded into giant H II regions and open clusters from the Milky Way using a comparative analysis of the evolution of their integrated photometric parameters in the colour–magnitude diagram (as it is shown in Figure 12). Here we use a catalogue of 650 the Milky Way OCs and compact associations (Kharchenko et al. 2005a,b, 2009).

The difference in mass distribution of the extragalactic SF regions and of the Milky Way OCs is explained by the fact that one is not able to observe small (faint) clusters in the remote galaxies. Masses of OCs in our Galaxy are within ≈ 10 to $\sim 10^5 M_\odot$, the lowest mass of young galactic clusters (ages < 10 Myr) is about $100 M_\odot$ (Piskunov et al. 2008).

Thus Figure 12 shows that extragalactic star clusters and the OCs in the Milky Way form a continuous sequence
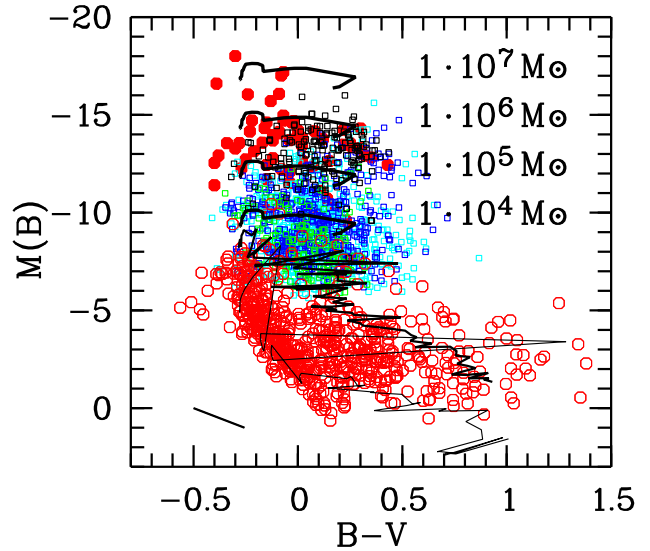
Figure 12. True colours and luminosities of star clusters (red filled circles) and colours and luminosities of star clusters corrected for the Galactic absorption and for the dust absorption due to the inclination of a galaxy (cyan, blue, green, and black dots), compared with the *Standard* mode of the SSP models (continuously populated IMF), and of OCs in the Milky Way (red open circles), compared with the *Extended* SSP mode (randomly populated IMF). We show the tracks of the *Standard* mode with an adopted characteristic metallicity of the studied star clusters of $Z = 0.012$, drawn in the age interval from 1 to 10 Myr as thick solid lines labelled with respective masses. Black fluctuating curves show the *Extended* mode tracks for typical metallicity of OCs ($Z = 0.019$) computed for the $3.2 \cdot 10^3 M_\odot$ (thick) and $150 M_\odot$ (thin) curves in the age interval from 1 Myr to 6.3 Gyr. The black straight line in the corner of the diagram is parallel to the extinction vector.

of luminosities (masses) and colours (ages). This diagram shows a hypothetical colour–magnitude diagram that will be observed in remote galaxies when the depth of present day extragalactic surveys is increased by 5–7 mag.

7 Summary

In this paper, we develop techniques for searching young unresolved star groupings (clusters, associations, and their complexes) and of estimating their physical parameters. We present a combination of spectroscopic and photometric data of the disc cluster population in spiral galaxies.

We present the following results:

1. The catalogue of photometric parameters for 1510 clusters (associations, complexes) younger 10 Myr in 19 galaxies.

2. Ages of 57, and masses of 63 out of 102 star clusters embedded in H II regions in 7 galaxies.

3. The derived masses of the observed extragalactic star clusters range from $10^4 M_\odot$ to $10^7 M_\odot$. More than 80% of them have masses in the range from 10^5 to $10^6 M_\odot$. The lowest mass estimate of $10^4 M_\odot$ for the objects in NGC 628 and NGC 6946 belongs to the mass interval of the youngest massive Galactic open clusters. This supports the idea on existance of single evolutionary sequence including both extragalactic star forming regions and Galactic OCs.

References

Ann, H.-B. & Kim, J.-M. 1996, JKAS, 29, 255–268.

Artamonov, B. P., Badan, Y. Y., Bruyevich, V. V., & Gusev, A. S. 1999, Astron. Rep., 43, 377–390.

Artamonov, B. P., Badan, Y. Y., & Gusev, A. S. 2000, Astron. Rep., 44, 569–578.

Artamonov, B. P., Bruevich, V. V., & Gusev, A. S. 1997, Astron. Rep., 41, 577–585.

Belley, J. & Roy, J.-R. 1992, ApJS, 78, 61–85.

Berg, D. A., Skillman, E. D., Croxall, K. V., Pogge, R. W., Moustakas, J., Johnson-Groh, M. 2015, ApJ, 806, A16.

Berg, D. A., Skillman, E. D., Garnett, D. R., Croxall, K. V., Marble, A. R., Smith, J. D. et al. 2013, ApJ, 775, 128.

Bertelli, G., Bressan, A., Chiosi, C., Fagotto, F., & Nasi, E., 1994, A&AS, 106, 275–302.

Bessell, M. S. 1990, PASP, 102, 1181–1199.

Bresolin, F., Kennicutt, R. C., & Garnett, D. R. 1999, ApJ, 510, 104–124.

Bressan, A., Marigo, P., Girardi, L., Salasnich, B., Dal Cero, C., Rubele, S., et al. 2012, MNRAS, 427, 127–145.

Brown, R. L. & Mathews, W. G., 1970, ApJ, 160, 939–946.

Bruevich, V. V., Gusev, A. S., Ezhkova, O. V., Sakhibov, F. K., & Smirnov, M. A. 2007, Astron. Rep., 51, 222–233.

Bruevich, V. V., Gusev, A. S., & Guslyakova, S. A. 2010, Astron. Rep., 54, 375–385.

Bruevich, V. V., Gusev, A. S., Guslyakova, S. A. 2011, Astron. Rep., 55, 310–323.

Cedrés, B., Cepa, J., Bongiovanni, Á., Castañeda, H., & Sánchez-Portal, M., Tomita A. 2012, A&A, 545, A43.

Dale, D. A., Cohen, S. A., Johnson, L. C., Schuster, M. D., Calzetti, D., Engelbracht, C.W. et al. 2009, ApJ, 703, 517–556.

Efremov, Y. N. & Elmegreen, B. 1998, MNRAS, 299, 588–594.

Elmegreen, B. G. & Efremov, Y. N. 1996, ApJ, 466, 802–807.

Elmegreen, B. G., Elmegreen, D. M., Salzer, J. J. & Mann, H. 1996, ApJ, 467, 579-588.

Epinat, B., Amram, P., & Marcelin, M. 2008, MNRAS, 390, 466-504.

Ferguson, A. M. N., Gallagher, J. S., & Wyse, R. F. G. 1998, AJ, 116, 673–690.

García-Benito, R., Díaz, A., Hägele, G. F., Pérez-Montero, E., López, J., Vílchez, J.M. et al. 2010, MNRAS, 408, 2234–2255.

Girardi, L., Bressan, A., Bertelli, G., Chiosi, C. 2000, A&AS, 141, 371–383.

Gusev, A. S. 2006a, Astron. Rep., 50, 167–181.

Gusev, A. S. 2006b, Astron. Rep., 50, 182–193.

Gusev, A. S. & Efremov, Y. N. 2013, MNRAS, 434, 313–324.

Gusev, A. S., Guslyakova, S. A., Novikova, A. P., Khramtsova, M. S., Bruevich, V. V. & Ezhkova, O. V. 2015, Astron. Rep., 59, 899–919.

Gusev, A. S. & Kaisin, S. S. 2002, Astron. Rep., 46, 712–720.

Gusev, A. S. & Kaisin, S.S. 2004, Astron. Rep., 48, 611–621.

Gusev, A. S., Myakutin, V. I., Sakhibov, F. K., & Smirnov, M. A. 2007, Astron. Rep., 51, 234–244.

Gusev, A. S., Park, M.-G. 2003, A&A, 410, 117–129.

Gusev, A. S., Pilyugin, L. S., Sakhibov, F., Dodonov, S. N., Ezhkova, O. V., Khramtsova, M. S. 2012, MNRAS, 424, 1930–1940.

Gusev, A. S., Sakhibov, F., Egorov, O. V., Shimanovskaya, E. V. & Shatsky, N. I. 2018, MNRAS (in preparation).

Gusev, A. S., Sakhibov, F., Piskunov, A. E., Kharchenko, N. V., Bruevich, V. V., Ezhkova, O. V. et al. 2016, MNRAS, 457, 3334–3355.

Gusev, A. S., Sakhibov, F. H. & Dodonov, S. N. 2013, Astrophys. Bull., 68, 40–52.

Gusev, A. S., Zasov, A. V., & Kaisin, S. S. 2003, Astron. Lett., 29, 363–371.

Gusev, A. S., Zasov, A. V., Kaisin, S. S., & Bizyaev, D. V. 2002, Astron. Rep., 46, 704–711.

James, P. A., Shane, N. S., Beckman, J. E., Cardwell, A., Collins, C. A., Etherton, J. et al. 2004, A&A, 414, 23–43.

Kaplan, S. A. & Pikelner, S. B. 1979, The physics of the interstellar medium, Nauka, Moscow (In Russian).

Kennicutt, R. C. Jr, Lee, J. C., Funes, J. G. J. S., Sakai, S., & Akiyama, S. 2008, ApJS, 178, 247–279.

Kharchenko, N. V., Piskunov, A. E., Röser, S., Schilbach, E., Scholz, R.-D. 2005a, A&A, 438, 1163–1176.

Kharchenko, N. V., Piskunov, A. E., Röser, S., Schilbach, E., Scholz, R.-D. 2005b, A&A, 440, 403–408.

Kharchenko, N. V., Piskunov, A. E., Röser, S., Schilbach, E., Scholz, R.-D., Zinnecker, H. 2009, A&A, 504, 681–688.

Knapen, J. H., Stedman, S., Bramich, D. M., Folkes, S. L., & Bradley, T. R. 2004, A&A, 426, 1135–1141.

Konstantopoulos, I. S., Bastian, N., Smith, L. J., Westmoquette, M. S., Trancho, G. & Gallagher, J. S., 2009, ApJ, 701, 1015–1031.

Kornilov, V., Kornilov, M., Voziakova, O., Shatsky, N., Safonov, B., Gorbunov, I. et al. 2016, MNRAS, 462, 4464–4472.

Lada, C. J. & Lada, E. A. 2003, ARA&A, 41, 57–115.

Landolt, A. U. 1992, AJ, 104, 340-371, 436-491.

Lang, K. R., 1978, Astrophysical Formulae. A Compendium for the Physicist and Astrophysicist, Springer-Verlag, Berlin, Heidelberg, New York.

Larsen, S. S. 1999, A&AS, 139, 393–415.

Larsen, S. S. 2004, A&A, 416, 537-553.

Larsen, S. S. & Richtler, T. 1999, A&A, 345, 59–72.

Marigo, P. & Girardi, L. 2007, A&A, 469, 239–243.

Marigo, P., Girardi, L., Bressan, A., Groenewegen, M. A. T., Silva, L., & Granato, G. L. 2008, A&A, 482, 883–905.

Márquez, I., Masegosa, J., Moles, M., Varela, J., Bettoni, D., & Galletta, G. 2002, A&A, 393, 389–407.

McCall, M. L., Rybski, P. M., & Shields, G. A. 1985, ApJS, 57, 1–62.

Osterbrock, D. E., 1989, Astrophysics of gaseous nebulae and active galactic nuclei, University Science Books, Mill Valley, CA.

Paturel, G., Petit, C., Prugniel, Ph., Theureau, G., Rousseau, J., Brouty, M. et al. 2003, A&A, 412, 45–55.

Piskunov, A. E., Kharchenko, N. V., Schilbach, E., Röser, S., Scholz, R.-D., & Zinnecker, H. 2008, A&A, 487, 557-566.

Piskunov, A. E., Kharchenko, N. V., Schilbach, E., Röser, S., Scholz, R.-D., & Zinnecker, H. 2011, A&A, 525, A122.

Regan, M. W., Thornley, M. D., Bendo, G. J., Draine, B. T., Li, A., Dale, D. A. et al. 2004, ApJS, 154, 204–210.

Reines, A. E., Nidever, D. L., Whelan, D. G., & Johnson, K.E. 2010, ApJ, 708, 26–37.

Rosales-Ortega, F. F., Diaz, A. I., Kennicutt, R. C., Sanchez, S. F. 2011, MNRAS, 415, 2439–2474.

Sakhibov, F. & Smirnov, M. A. 1990, Soviet Astronomy, 34, 236–238.

Sánchez, S. F., Rosales-Ortega, F. F., Marino, R. A., Iglesias-Páramo, J., Vílchez, J. M., Kennicutt, R. C. et al. 2012, A&A, 546, A2.

Scalo, J. M. 1986, Fundamentals of Cosmic Physics, 11, 1.

Schmitt, H. R., Calzetti, D., Armus, L., Giavalisco, M., Heckman, T. M., Kennicutt, R. C. Jr et al. 2006, ApJS, 164, 52–80.

van Zee, L., Salzer, J. J., Haynes, M. P., O'Donoghue, A. A., & Balonek, T.J. 1998, AJ, 116, 2805–2833.

Whitmore, B. C., Chandar, R., Kim, H., Kaleida, C., Mutchler, M., Stankiewicz, M., et al. 2011, ApJ, 729, 78.

Young, J. S., Allen, L., Kenney, J. D. P., Lesser, A., & Rownd, B. 1996, AJ, 112, 1903–2378.